

Below this barren interval, Sample 181-1122C-55X-CC yields assemblages characteristic of middle Miocene age. We surmise that a major hiatus separating the lower Pliocene from the middle Miocene occurs between Samples 181-1122C-55X-CC (499.7 mbsf) and 53X-CC (477.8 mbsf), at around 490 mbsf. The samples immediately below the unconformity are characterized by the occurrence of a moderately preserved assemblage containing *Calcidiscus premacintyreii*, *Coccolithus miopelagicus*, and medium-sized *Reticulofenestra* spp. Although these species occur also in samples above this unconformity as a result of reworking, they occur in large quantities with better preservation below this level. The top of the sequence below the unconformity is estimated to be older than 10.9 Ma, based upon the appearance of *Coccolithus miopelagicus* (Gartner, 1992).

The middle Miocene section (499.7–617.8 mbsf) contains a few badly preserved *Discoaster* spp. The general paucity of major marker species hampers our effort to correlate the sequence with Martini's (1971) zonation. Nevertheless, several constraints can be given: (1) the bottom of the deepest core contains *Calcidiscus premacintyreii*, which indicates an age younger than 17.4 Ma (Gartner, 1992); (2) Sample 181-1122C-60X-CC (541.1 mbsf) marks the FO of *Calcidiscus macintyreii*, which indicates a middle Miocene age of 12.34 Ma (Raffi and Flores, 1995); and (3) the LO of *Sphenolithus heteromorphus* (dated 13.52 Ma, Raffi and Flores, 1995) in Sample 181-1122C-62X-CC (563.3 mbsf) gives another constraint to bracket the interval into the middle Miocene. In summary, nannofossil assemblages suggest that the lower quarter of the core (499.7–617.8 mbsf) was deposited between 17.4 and 10.9 Ma.

### Foraminifers

The uppermost part of Site 1122 is late Pleistocene to Holocene in age (0–0.45 Ma), based on the sporadic presence of *Globorotalia hirsuta* (Samples 181-1122B-1H-CC, 181-1122A-7H-CC, and 181-1122A-11X-CC). Many high spiro-conical globorotaliids, with features similar to those in *Globorotalia hirsuta* and *G. praehirsuta*, occur in Samples 181-1122C-30X-CC and 31X-CC, but they are here considered to be precursors of true *G. hirsuta* populations and are not indicators of a similar late Pleistocene age (Tables T5, T6).

*Globorotalia inflata* is the dominant unkeeled globorotaliid from the top of the section down to Sample 181-1122C-34X-CC, where it is replaced in dominance by *Globorotalia puncticuloides*. In other parts of the region, this datum has been estimated to be ~0.9 Ma (Hornibrook and Jenkins, 1994). At Site 1122, this datum lies ~10 m above the Brunhes/Matuyama boundary (0.78 Ma), indicating that the previously estimated level may be a little too old. As in other stratigraphic sections in this region (e.g., DSDP Site 594 and Site 1119), *Globorotalia truncatulinoides* is sporadic and small when it first appears close to the FCO of *Globorotalia inflata* (in Sample 181-1122C-26X-2, 7–8 cm, well above the Brunhes/Matuyama boundary). Similarly, the age of the FO *G. truncatulinoides*, previously estimated for this region at ~0.9 Ma, is possibly also a little early.

Assemblages with unkeeled globorotaliids dominated by *G. puncticuloides* (3.6–0.7 Ma) and with common *Globorotalia crassula* (2.6–0 Ma) extend down to Sample 181-1122C-31X-CC and indicate a late Pliocene to early Pleistocene age for this section. Unaccompanied *G. puncticuloides* extends down to Sample 181-1122C-51X-CC and indicates that

---

T5. Identification and abundance of planktonic foraminifers, p. 120.

---



---

T6. Identification and abundance of benthic foraminifers, p. 121.

---

this interval is no older than ~3.6 Ma (middle Pliocene). Sample 181-1122C-53X-CC contains the LO *Globorotalia puncticulata* (3.7 Ma).

No planktonic foraminifers or age-specific benthic forms are present in Samples from 181-1122C-54X-CC to 57X-CC, nor from 1122C-59X-CC to 61X-CC, with the exception of a 7-cm whitish marl interval in otherwise brown-green clay at 181-1122C-55X-4, 22–24 cm. The assemblage in the latter sample is a fine silt fraction (~60  $\mu\text{m}$ ) foraminifer ooze, exclusively composed of cold water–mass taxa, including *Globigerina quinqueloba* and *Neogloboquadrina pachyderma* (FO ~11.3 Ma). The assemblage is undoubtedly winnowed, either from current erosion or suspension separation in a gravity flow. A small assemblage in Sample 181-1122C-58X-CC contains several *Globorotalia miotumida* (FO 13.2 Ma), numerous *Neogloboquadrina continuosa* (LO ~11 Ma), and *Paragloborotalia mayeri* (LO 10.8 Ma), indicating a late middle Miocene age (11–13.2 Ma, late Lillburnian–Waiauian Stages).

Sample 181-1122C-62X-CC heralds a return of planktonic foraminifers and contains *Globorotalia praemenardii* (LO ~13.2 Ma), *G. conica* (LO ~13 Ma), and one *Orbulina suturalis* (FO 15.1 Ma). These indicate a middle Miocene age (15–13.2 Ma, Lillburnian Stage). The evolutionary transition from *Globorotalia miozea* to *G. praemenardii* occurs in Sample 181-1122C-63X-CC, indicating an early middle Miocene age (~15.8 Ma, Clifdenian Stage). The lower 40 m of the hole extends back across the early to middle Miocene boundary, with the lowest Sample (181-1122C-68X-CC) containing numerous five-chambered *Globorotalia miozea* (FO 16.7 Ma), one *Globigerinoides bisphericus* (FO 17 Ma), and the first good specimens of *Globorotalia zealandica* (LCO 16.7 Ma), indicating a late early Miocene age (~16.7 Ma, mid- to late Altonian Stage) for the bottom of Hole 1122C.

## Diatoms

Diatoms are present nearly throughout the whole recovered sequence except for the lowermost 34 m, which is characterized by silica diagenesis that led to dissolution of diatoms and formation of authigenic zeolites. In the cores above, preservation of diatoms varies (Table T7).

The upper Pleistocene sequence of turbidites is dominated by autochthonous, planktonic diatoms of the Bounty Trough surface waters, whereas the early Pleistocene turbidite and Pliocene contourite deposits below are dominated by reworked older diatoms from the Pliocene, Miocene, and Paleogene.

In the upper Pleistocene turbiditic sequence, down to the Brunhes/Matuyama boundary (i.e., 0–300 mbsf), autochthonous, planktonic diatoms provide three datums: the well-dated late Pleistocene shifts in abundance of *Hemidiscus karstenii* and *Actinocyclus ingens* and also the last occurrence of *Thalassiosira elliptipora* (Figs. F16, F17; Tables T7, T8; and Table T4, p. 63, in the “Explanatory Notes” chapter).

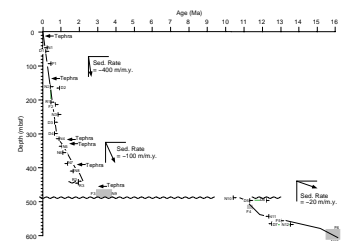
For the deposits below, a comparison with the biostratigraphic results from calcareous nannofossils, foraminifers, and the paleomagnetic reversal record showed that in the interval from Sample 181-1122B-52X-CC to 62X-CC (470 to 570 mbsf), the occurrences of *Denticulopsis dimorpha* (10.1–10.7 to 12.2 Ma) and *Simonseniella barboi* (1.2–1.8 to 12.5 Ma) fit with the middle Miocene age determined by these other methods. Here the planktonic foraminifers are also better preserved and more diverse, which suggests that this is a period of higher sedimentation rates, resulting in the preservation of at least the more robust

---

T7. Identification and abundance of diatoms, p. 123.

---

F17. Age-depth curve for Hole 1122C, p. 58.




---

T8. Age of events in Ma, p. 127.

---

autochthonous planktonic diatoms. In the contourite sediments above and below (300–470 mbsf and 570 mbsf to core base), age-diagnostic, autochthonous diatoms cannot be found and dissolution-resistant reworked diatoms from Eocene and Oligocene strata are present (see discussion under paleoenvironment).

### Radiolarians

The radiolarian biostratigraphy at Site 1122 is based on the examination of 81 core-catcher samples (Table T9). Throughout the turbidite and contourite units, radiolarians are sporadic and occur very rarely. However, radiolarian faunas in twenty samples are moderately well-preserved and provide useful age and paleoenvironmental information. Most samples between 0 and 402 mbsf yield common to abundant *Antarctissa denticulata*, *Antarctissa strelkovi*, *Lithelius nautiloides*, and *Saccospyris antarctica*, which represent subantarctic waters. The lower sandy units (>452 mbsf) are almost barren, except for Samples 181-1122B-62X-CC and 63X-CC.

The uppermost interval between Samples 181-1122C-1H-CC and 17X-CC (0–133 mbsf) is of late Pleistocene age (younger than 0.46 Ma), based on the LO of *Stylatractus universus* (0.46 Ma) in Sample 181-1121C-18X-CC (140.5 mbsf). This datum is well known and well established worldwide; however, in this section, *Stylatractus universus* occurs only sporadically. Rare, reworked forms of middle to upper Miocene species like *Cyrtocapsella japonica*, *C. tetrapera*, *Stichocorys peregrina*, and *Eucyrtidium calvertense* were observed in the upper part of the section.

Samples 181-1122C-48X-CC and 49X-CC yield common *Eucyrtidium calvertense* (LO 1.92 Ma) and 49X-CC also contains *Lithelius nautiloides* (FO 1.93 Ma). Therefore, the interval between 181-1122C-18X-CC and 48X-CC (140.5–432.4 mbsf) is dated as latest Pliocene to late Pleistocene (0.46–1.9 Ma). The FO datum of *Lithelius nautiloides* is apparently too high, resulting from reworking, because samples below 444 mbsf were barren or contained only rare radiolarians. Samples 181-1122C-62X-CC and 63X-CC yield common radiolarians including *Calocycletta* sp., *Lychnocanoma* sp., and *Cyrtocapsella tetrapera* of Miocene age.

## Paleoenvironment

### Foraminifers

In the upper Pliocene–Quaternary section (Cores 181-1122A-1H to 181-1122C-53X; 0–478 mbsf), lithostratigraphic Subunits IA through IC consist of turbidite beds of graded, very fine sand to silt (“coarse beds”), deposited on the Bounty Channel levee by periodic turbidity currents, which are interbedded with thin beds of hemipelagic to pelagic mud (“fine beds”) deposited from suspension during the intervening periods (Fig. F18).

Samples from the “fine beds” (e.g., Samples 181-1122A-3H-CC, 181-1122C-25X-CC, and 181-1122C-26X-2, 7–8 cm) have planktonic forms composing ~80%–98% of the foraminifers. The benthic foraminiferal assemblage (Table T6) is dominated by typical upper abyssal calcareous assemblages containing varying mixtures of fairly small *Trifarina angulosa*, *Epistominella exigua*, *Melonis barleeanum*, *Cassidulina carinata*, *Cibicides pachyderma*, *Oridorsalis umbonatus*, *Pyrgo murrhina*, *Quinqueloculina venusta*, and *Globocassidulina subglobosa*. The fine beds also contain a

T9. Identification and abundance of radiolarians, p. 128.

F18. Summary of changing foraminiferal faunas, p. 59.

Lithostratigraphic Unit	Planktonic Fauna	Benthic Fauna		
UNIT I c o a x D	Turbidite (ungraded)	Normal, well-preserved, oceanic fauna	Deep-water assemblage with addition of small shelf and bathyal forms	Pliocene-Pleistocene
		Normal, well-preserved, oceanic fauna	Only deep-water assemblage	
UNIT II A B	Contourite (dominated)	Large, thick-walled, oceanic fauna, few or no small forms	Only deep-water assemblage	Dissolution
		Barren or rapidly buried fauna of small forms (reworked) + minor reworked Oligocene	Barren or only deep-water assemblage	
UNIT III A B	Deline fine beds and coarse turbidites	Variable oceanic fauna	Only deep-water assemblage	Miocene
		Normal oceanic fauna	Dominantly mid-shelf fauna (large and small) with minor deep-water assemblage	

few, small, shallow-water, benthic forms derived from “inner and mid-shelf depths (e.g., *Elphidium advenum* and *E. charlottense*).

Samples from the “coarse beds” (e.g., Samples 181-1122A-7H-CC, 9X-CC, and 12X-CC) have planktonic forms comprising 75%–90% of the foraminifers. The benthic foraminiferal assemblage is dominated by small (mostly <0.2 mm) *Elphidium advenum*, *E. charlottense*, *Uvigerina dirupta*, *Miliolinella subrotundata*, *Nonionellina flemingi*, *Notorotalia*, and *Pileolina* spp. apparently displaced in with the turbiditic sand from “shelf” depths, and mixed with other deeper water bathyal or abyssal forms (e.g., *Trifarina angulosa*, *Melonis* spp., *Pullenia bulloides*, large *Globocassidulina* spp., and *Nuttallides umbonifera*) that may have either been picked up en route or have lived in the turbiditic sediment after it was deposited on the levee. The benthic foraminifers in these turbidites thus exhibit a mixed origin from inner shelf depths (e.g., *Pileolina* spp. and *Zeaflorilus parri*) through to abyssal.

The Quaternary planktonic foraminiferal assemblages in lithostratigraphic Unit I are dominated by a mix of small *Neogloboquadrina pachyderma*, *Globigerina quinqueloba*, larger *Globigerina bulloides*, *Globorotalia inflata*, and lower in the interval by *Globorotalia puncticuloides* and *G. crassula*. Some samples have a cooler water aspect with a greater dominance of small *N. pachyderma* and *G. quinqueloba* (e.g., Samples 181-1122C-26X-CC and 34X-CC); others have a slightly warmer aspect with the addition of a moderate number of large *Orbulina universa*, *Globorotalia crassula*, and *G. hirsuta*, and a greater percentage of large *Globorotalia inflata* or *G. puncticuloides* (e.g., Samples 181-1122A-7H-CC, 181-1122C-16X-CC, and 181-1122C-20X-CC).

In the lower part (lithostratigraphic Subunit IIA) of the Pliocene–Quaternary section (from Samples 181-1122C-47X-CC to 53X-CC), most of the planktonic assemblages are sparse and mainly composed of bigger, thicker-walled specimens with only a few, small, thin-walled forms present. It would seem that the planktonic assemblage is being affected by dissolution, with only the thicker-walled specimens and a few rapidly buried thinner-walled ones not being dissolved. The assemblages suggest that the Carbonate Compensation Depth (CCD) was possibly at a slightly higher level during this period than it was later in the Quaternary. Alternatively, corrosive cold-water flow may have been active.

The Miocene section (Cores 181-1122C-54X to 68X, 488 to 618 mbsf) contained foraminiferal assemblages that are predominantly partly recrystallized and poorly to moderately preserved. In the upper half of the interval (lithostratigraphic Subunit IIB), many of the fine sands are barren of foraminifers (e.g., Samples 181-1122C-54X-CC, 56X-CC, 59X-CC, and 61X-CC).

A light mud (Sample 181-1122C-55X-4, 22–24 cm) from this largely barren interval contains a rich assemblage of extremely small planktonic and benthic foraminifers, the result of winnowing from currents or suspension separation in a gravity flow. Its low-diversity planktonic assemblage with *Neogloboquadrina pachyderma* and *Globigerina quinqueloba* indicates cool water above. This sample also contains evidence (two minute specimens of *Chiloguembelina*) of reworking from Oligocene oceanic strata. A similar assemblage of dominantly small planktonic forms occurs in Sample 181-1122C-55X-CC, together with a sparse assemblage of deep-water benthic foraminifers, which is dominated by large *Nodosaria longiscata* and frequent *Oridorsalis umbonatus*.

Sample 181-1122C-55X-CC contains no planktonic foraminifers and a sparse deep-water benthic assemblage (e.g., *Bolivinospis*, *Cibicidoides*

*pachyderma*, *Eggerella bradyi*, *Globocassidulina subglobosa*, *Laticarinina pauperata*, *Melonis pompilioides*, and *Oridorsalis umbonatus*). We conclude that the site was below the CCD and that all planktonic foraminifers dissolved before they settled on the bottom, whereas the benthic forms were preserved by rapid burial.

Foraminiferal assemblages are present throughout the lower half (lithostratigraphic Unit III) of this Miocene interval and contain rich, planktonic assemblages with a wide range of sizes. Temperate overhead water is indicated by the abundance of forms from the *Globorotalia miozea* and *Globorotalia zealandica* lineages. The almost total absence of orbulines argues against any subtropical influence.

Entirely deep-water benthic assemblages are present in Samples 181-1122C-62X-CC and 63X-CC (lithostratigraphic Subunit IIIA), but below this in Subunit IIIB there is a substantial component of “mid-shelf” (~50–100 m depth) benthic foraminifers. These benthic forms appear to be of similar age as the deep-water assemblage to which they have been added, although a late Oligocene or early Miocene age cannot be entirely ruled out. The unusual aspect of these allochthonous shallow-water benthic assemblages is the large size of many specimens (>0.25 mm) and their abundance (composing up to 90% of the benthic assemblage in Samples 181-1122C-66X-CC and 67X-CC). Although abrasion and breakage is evident in some specimens, others still have crisply preserved ornament and show little rounding. This suggests downslope transport by mass-flow mechanisms and no long-distance transport by strong bottom currents. The shallow-water assemblage is dominated by varying mixtures of *Notorotalia spinosa* and *Nonionella novozealandica*, a well-known New Zealand, lower Miocene association from middle shelf depths (~50–100 m). Other shallow-water components include *Anomalinoides fasciatus*, *A. macraglabra*, *Cibicides perforatus*, *C. notocenicus*, *Discorotalia tenuissima*, *Elphidium advenum*, *Kolesnikovella australis*, *Melonis maorica*, and *Siphonina australis*.

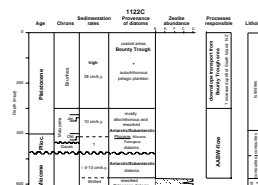
Thus the lower half (lithostratigraphic Subunit IIIB) of the Miocene interval has an allochthonous, planktonic-dominated assemblage that accumulated at similar abyssal depths as today and a large component of mostly benthic foraminifers derived from middle shelf depths.

## Diatoms and Silica Diagenesis

In the upper Pleistocene section, the diatom assemblages are a mix of subantarctic and cosmopolitan, planktonic species with an additional input of local neritic and shallow-water species from the Bounty Trough head. The diatom valves are well preserved because of the high sedimentation rates of fine-grained, clastic terrigenous material. The sediment facies is mainly turbidites interbedded with thin hemipelagic sediments. The characteristic occurrence of diatom assemblages within these turbidites is that no diatoms are found in the quartz sand at the turbidite bases, whereas higher in the clayey part of the turbidite, autochthonous, planktonic diatoms occur together with species typical for more nearshore areas and with benthic diatoms, which must be derived from shallow, coastal areas. With the transition to nonturbidite sediments, these dislocated shallower water diatoms decrease in abundance.

The provenance of the diatoms is different in the underlying early Pleistocene turbiditic sequence and the Miocene–Pliocene contourite sediments (below 300 mbsf; Fig. F19), the latter being shaped by Antarctic Bottom Water (AABW). The average sedimentation rates deter-

F19. Provenance of diatoms in the Neogene, p. 60.



mined for these sediments are considerably lower than for the upper Pleistocene turbidite sequence above: approximately one-quarter lower for the lower Pleistocene turbiditic sequence and one-eighth to one-quarter lower for the contourite deposits. Here, only the relatively dissolution-resistant diatom valves are preserved. In these sediments, subantarctic/Antarctic diatoms of Pliocene and Miocene age are found as well as reworked Eocene–Oligocene species. Except for the middle Miocene section mentioned above, where the ages derived from diatoms agree with those derived from the calcareous microfossils, a large part of the assemblage has to be considered allochthonous or reworked, brought in by AABW.

The changing sedimentation rates and the changing provenance of the diatoms indicate that the dominating influence of the AABW, which is characteristic through most of the Neogene sediments at this site, is overcome by turbidite sedimentation during the late Pleistocene. This change in sedimentation rate and provenance of diatoms may reflect an increased late Pleistocene uplift of South Island New Zealand, which has been reported to reach 6 mm/yr for the Marlborough ranges (e.g., van Dissen and Yeats, 1991).

### Radiolarians

Upper Pliocene to Pleistocene radiolarian faunas obtained from the section (Cores 181-1122A-1H to 181-1122C-49X) are characterized by the consistent occurrences of abundant *Antarctissa denticulata*, *Antarctissa strelkovi*, *Cycladophora davisiana davisiana*, *Lithelius nautiloides*, and *Saccospyris antarctica*. These species are representative of Antarctic/subantarctic affinity. In addition, there is common to abundant occurrence of *Cycladophora davisiana davisiana* in Samples 181-1122A-1H-CC, 181-1122A-6H-CC, 181-1122B-1H-CC, 181-1122C-14X-CC, and 181-1122C-35X-CC. It is well known that the relative abundance curve of *Cycladophora davisiana* corresponds well with oxygen isotope curve (Morley and Hays, 1979).

## PALEOMAGNETISM

Core archive-halves from Holes 1122A and 1122C were measured on the shipboard pass-through cryogenic magnetometer. Declination, inclination, and intensity of natural remanent magnetization (NRM) and 20-mT alternating field (AF) demagnetization steps were measured at 5-cm intervals. The first few cores of each hole were also measured at a 10-mT demagnetization step; this step added little extra information and, because of time constraints, only the 20-mT step was continued. In situ tensor tool data were collected for Cores 181-1122A-3H through 8H and 181-1122C-3H through 13H. Tensor tool data were good for APC cores from Hole 1122C, but a problem with the shipboard pass-through cryogenic magnetometer prevented the use of declination for polarity determination in the APC cores. Therefore, only inclination could be used to determine magnetic polarity of Holes 1122A and 1122C. At least two discrete oriented samples were collected from the working half of each core interval for progressive AF and thermal demagnetization and rock magnetic studies. Whole-core magnetic susceptibility was measured on all cores using a Bartington susceptibility loop on the automated multisensor track (MST). For the purposes of this initial report, only Hole 1122C is discussed in detail below.

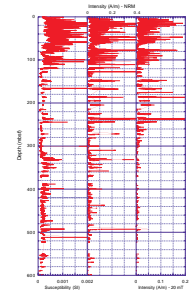
Magnetic susceptibility and intensity of magnetic remanence define several zones of magnetic behavior in Hole 1122C (Fig. F20). The upper 110 mbsf have high susceptibility ( $0.5^{-1} \times 10^{-3}$  SI) and high intensity of magnetic remanence. NRM values averaged 0.1–0.2 A/m and dropped only slightly to 0.05–0.1 A/m after 20 mT of AF demagnetization. Between 110 and 260 mbsf, average susceptibility values dropped to  $2 \times 10^{-4}$  SI, but average remanence values remained high for both NRM and 20-mT levels. Beneath 260 mbsf, susceptibility and remanence values were both low ( $2 \times 10^{-4}$  SI and  $10^{-4}$  A/m, respectively), except for the interval between 320 and 360 mbsf in the vicinity of two tephra horizons, where susceptibility and NRM values increased to  $5 \times 10^{-4}$  SI and  $8 \times 10^{-2}$  A/m respectively. These zones defined by magnetic susceptibility and intensity of remanence are roughly equivalent to lithologic changes in the core (see “Lithostratigraphy,” p. 4).

**Paleomagnetic Behavior and Rock Magnetism**

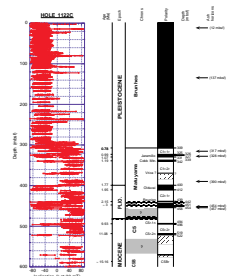
NRM measurements displayed consistent, steeply positive (down-core) inclinations ranging between  $+70^\circ$  and  $+80^\circ$ , consistent with a drill-string overprint induced during coring. The single 20-mT AF demagnetization step proved very effective in removing the overprint and elucidating a polarity reversal stratigraphy (Fig. F21). Intensity of magnetization was strong enough that discrete samples could be subjected to stepwise AF demagnetization up to 80 mT in the shipboard pass-through cryogenic magnetometer (Fig. F22). The drilling-induced overprint was only observed in reversed polarity samples (e.g., Fig. F22A, F22B, F22G, F22H, F22I), and it only accounted for a very small percentage of the NRM intensity. Further stepwise AF demagnetization demonstrated that all samples had reached a stable primary remanence direction by 20 mT of demagnetization (Fig. F22). Several samples from Hole 1122C demonstrate radial remagnetization from demagnetization attempts with AF fields above 50 mT (e.g., Fig. F22B, F22C). Figure F23 shows acquired isothermal remanence magnetizations (IRM) to saturation (SIRM) and backfield SIRM. Most of the samples subjected to SIRM are magnetically “soft” and were saturated by an applied field of 300 mT. However, samples from 450–580 mbsf did not saturate fully until applied fields were above 700 mT (Fig. F23C). Despite this difference in SIRM, coercivity of remanence ( $B_{cr}$ ) was between 25 and 75 mT in all cases. Samples from between 300 and 400 mbsf are particularly uniform in rock magnetic character, with an SIRM of 300 mT and  $B_{cr}$  of 25 mT. AF and thermal demagnetization of the SIRM demonstrates two types of behavior caused by variations in magnetic mineralogy and magnetic grain-size. Samples from the upper 200 mbsf of Hole 1122C have very low unblocking temperatures ( $350^\circ$ – $400^\circ\text{C}$ ) and “soft” but distributed coercivity spectra (Fig. F24A, F24B). Beneath 200 mbsf, unblocking temperatures are mostly higher ( $\sim 600^\circ\text{C}$ ) (Fig. F24C, F24E, F24F).

The “soft” SIRM, low  $B_{cr}$ , distributed unblocking temperatures up to  $\sim 600^\circ\text{C}$ , and distributed coercivity spectra demonstrate that magnetite of distributed grain size is the main carrier of remanence in samples from beneath 200 mbsf in Hole 1122C. In each case a secondary component of magnetization is clear, from a variable but small loss of intensity between  $320^\circ$  and  $360^\circ\text{C}$  in the unblocking temperature spectra (Fig. F24C, F24E, F24F). This may be a result of the presence of sulfide minerals, which, in turn, may also explain the slight “hardness” of SIRM acquisition in some cases (Fig. F23). Above 200 mbsf, however,

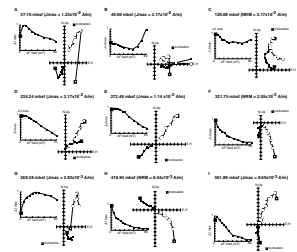
F20. Magnetic susceptibility and NRM intensity from Hole 1122C, p. 61.



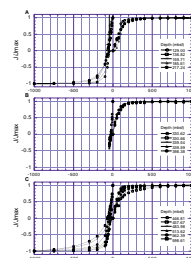
F21. Whole-core inclination and polarity interpretation of Hole 1122C, p. 62.



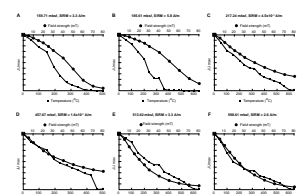
F22. Vector component diagrams of AF demagnetization behavior, p. 63.



F23. Isothermal remanent magnetization, p. 64.



F24. Plots of normalized intensity of magnetization, p. 65.



the carrier of magnetic remanence is more difficult to isolate. The low unblocking temperatures rule out magnetite as a magnetic carrier and suggest that a sulfide mineral might be the sole carrier of remanence. However, the IRM acquisition curve is saturated at low applied fields (Fig. F23A), and  $B_{cr}$  values are between 50 and 75 mT.

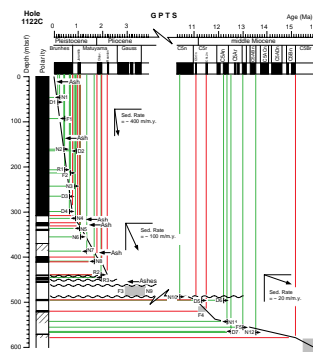
### Magnetostratigraphy

After 20 mT of demagnetization, the inclination record from Hole 1122C is well defined and allows a clear pattern of magnetic polarity to be established (Fig. F21). Two zones of characteristic polarity behavior are identified: above 309 mbsf, polarity is normal except for short excursions that do not have fully reversed inclinations. Beneath 309 mbsf, polarity alternates between normal and reversed intervals but is dominantly reversed. In the XCB cores (beneath 110 mbsf), polarity interpretation is complicated by the low recovery. It was not possible to determine a characteristic polarity pattern beneath 520 mbsf. Despite poor recovery, most of the polarity transitions occur in recovered intervals rather than in “core breaks.” Furthermore, polarity transitions occur within intervals of continuous sedimentation rather than at stratigraphic breaks identified in the core (see “Lithostratigraphy,” p. 4). Several key biostratigraphic datum events (see “Biostratigraphy,” p. 13) define a unique correlation between the magnetic polarity record of Hole 1122C and the Geomagnetic Polarity Time Scale (GPTS) (Berggren et al., 1995; Cande and Kent, 1995) (Fig. F25).

The uppermost 309 mbsf of Hole 1122C is of normal polarity and the last occurrences (LO) of *Globorotalia punctulinoidea* (F2, 0.7–0.8 Ma), *Actinocyclus ingens* (D3, 0.64 Ma), and *Thalassiosira elliptipora* (0.65–0.7 Ma) at 213, 265, and 300 mbsf, respectively, suggest that this interval is entirely within the Brunhes normal chron (C1n). Several short excursions are recognized above 309 mbsf (Fig. F21). These may correlate with intervals of depressed NRM and 20-mT intensity (Fig. F20). Further paleomagnetic and dating work may define them well enough to correlate with polarity excursions known from high-resolution terrestrial records (e.g., Worm, 1997) and high-resolution marine intensity records from the equatorial regions (e.g., Meynadier et al., 1995).

Between 309 and 487 mbsf, nannofossils provide the key datums for correlation (Fig. F25). The FO of *Gephyrocapsa parallela* (0.95 Ma, N4) and *Reticulofenestra asanoi* (1.06 Ma, N5) confine the mainly reversed polarity with short normal polarity intervals, between 309 and 350 mbsf to the upper part of the Matuyama Chron (C1r). The normal polarity intervals between 325 and 331 mbsf are correlated with the Jaramillo Subchron (C1r.1n) and the lower normal polarity event (339–342 mbsf) is correlated with the Cobb Mountain Event. Between 342 and 442 mbsf the normal-reversed-normal-reversed (N-R-N-R) polarity pattern is correlated with the lower part of the Matuyama Chron. The occurrence of *Gephyrocapsa* (large) (N6–N7, 1.1–1.36 Ma) between 356 and 388 mbsf and the FO of *Gephyrocapsa* (medium) (N8, 1.66 Ma) at 410 mbsf confines the uppermost reversed polarity interval of the N-R-N-R pattern to Subchron C1r.2r. A short excursion at ~370 mbsf may correlate with the Vrca or younger Olduvai Subchron (Baksi, 1995). Two radiolarian datums (LO *Lithelius nautiloidea*, 1.93 Ma and FO *Eucyrtidium calvertense*, 1.92 Ma) confine the remaining N-R-N pattern to Subchrons C2r.1n (Reunion Subchron), C2r.1r, and Chron C2n (Olduvai Chron), respectively.

F25. Age model and correlation of Hole 1122C magnetic polarity zonation, p. 66.



Foraminifer (F3) and nannofossil (N9) faunas beneath 461 mbsf suggest that a disconformity at this level separates the underlying lower Gauss Chron-age strata from the overlying Matuyama Chron-age strata. At 487 mbsf, all microfauna and microflora identify a major stratigraphic disconformity with underlying strata of middle Miocene age (see “**Biostratigraphy**,” p. 13). Magnetic polarity stratigraphy in this interval (442–487 mbsf) suggests an even more complex situation, with additional stratigraphic discontinuities, as the Gauss Chron (C2An) is of mostly normal polarity, yet in Hole 1122C the magnetic polarity at this level is mostly reversed. Beneath the disconformity at 487 mbsf, foraminifers (*Neogloboquadrina continuosa*, *N. pachyderma*, and LO of *Gr. praemenardii*, F5), nannofossils (LO *Coccolithus miopelagicus*, N10, FO *Calcidiscus macintyreii*, N11, and LO *Sphenolithus heteromorphus*, N12), and diatoms (LO of *Denticulopsis dimorpha*, D6, and FO *Simonseniella barboi*, D7) all suggest that the interval between 487 and ~575 mbsf ranges in age between 10 and 12.5 Ma. A characteristic magnetic polarity reversal pattern of two short normal events within an interval of reversed polarity allows better definition of age as Chron C5r is the only distinct interval of reversed polarity in this section of the GPTS. Chron C5r contains two short normal polarity subchrons (C5r.1n and C5r.2r) that are correlated with the two short normal polarity intervals at 494–496 mbsf and 519–522 mbsf, respectively. Foraminifers (co-occurrence of *Gr. zealandica* and *Gr. miozea*, F6) and the LO of the nannofossil *C. premacintyreii* (N13) suggest that the base of Hole 1122C is older again (~16–17 Ma). The basal 20 m of the hole is of reversed polarity and may correlate with Chron C5Br. However, poor recovery makes this correlation uncertain.

From the age model presented in Figures F21 and F25, average sedimentation rates are on the order of 400 m/m.y. for Subunits IA, IB, and IC (see “**Lithostratigraphy**,” p. 4) and 100 m/m.y. for Subunits ID and IIA. Average sedimentation rates could not be determined accurately for the lowermost part of Hole 1122C (lithostratigraphic Subunits IIB, IIIA, and IIIB) although they are likely to be an order of magnitude lower (~20 m/m.y.; Fig. F25). Tephra were identified at seven horizons in Hole 1122C (Figs. F21, F25; see “**Lithostratigraphy**,” p. 4). Dating of these will provide important additional information to help refine the magnetobiostratigraphic age model presented here. The tephra at 12 mbsf has already been identified as the Kawakawa Tephra (Carter et al., 1995). Using the average sedimentation rates from above and the stratigraphic position of the remaining tephra horizons, the following correlations with tephra reported from onland studies in New Zealand are possible: the tephra at 137 mbsf may correlate with the Rangitawa Tephra (Pillans et al., 1996); and the tephra at 317, 328, and 390 mbsf with the Kaukatea, Potaka, and Pakihikura Tephra, respectively (Pillans et al., 1994). Dating of the two tephra at 454 and 457 mbsf will provide important constraints on this interval of Hole 1122C, as the age is, as yet, poorly constrained.

### Environmental Magnetism

Differences in susceptibility and intensity of magnetic remanence (NRM and 20 mT), combined with magnetic mineralogical variations (identified by IRM, SIRM, and AF and thermal demagnetization behavior), demonstrate changes in the magnetic character at depth in Hole 1122C from changes in sedimentologic processes and sources. It is clear that in Unit I the susceptibility record is driven primarily by the sandier

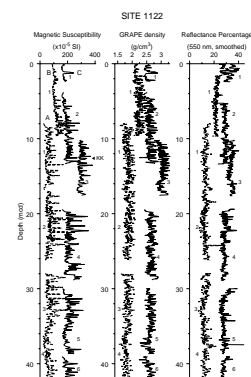
interbeds of the turbidite sequence, whereas the intensity of magnetic remanence is held by similar minerals of similar grain size in both the sandy and muddy interbeds. Such a record suggests a preferential loss of the coarser sediments in the XCB coring process as compared with APC coring where both coarse- and fine-grained interbeds are recovered. A change in intensity of remanence (at 20 mT of demagnetization) is noted beneath ~260 mbsf. This is coincident with the boundary between lithostratigraphic Subunits IC and ID. Thermal demagnetization experiments show that this is most likely because of a change in magnetic mineralogy. An increase in fine-grained magnetite beneath 260 mbsf suggests a possible change in sediment source. Variations in intensity of magnetic remanence in the upper 100 mbsf of Hole 1122C (Fig. F20) suggests fluctuations in sedimentation rates not recognized in the lithostratigraphic record and/or variations in intensity of the geomagnetic field at time of deposition.

### COMPOSITE DEPTHS

A composite section for Site 1122, constructed using data from Holes 1122A, 1122B, and 1122C, yielded overlapping records for the upper ~83 meters composite depth (mcd). At least one gap in continuity exists in this composite record at ~73 mcd. Three high-resolution data sets proved useful for correlation at this site: magnetic susceptibility (MS) and gamma-ray attenuation porosity evaluator (GRAPE), both measured on whole cores on the MST, and spectral reflectance at 550 nm (the center wavelength of the range measured), measured on split cores. The wavelength of variation in natural gamma-ray intensity (NGR) is too broad to be useful for hole-to-hole correlation at this site. Magnetic susceptibility proved the most reliable measurement for correlation, whereas GRAPE and reflectance records primarily provided confirmation of ties. Exceptions are (1) ties from Cores 181-1122C-3H to 181-1122A-2H and from 181-1122C-4H and 181-1122A-3H, both based on GRAPE density records, and (2) the correlation between Cores 181-1122B-1H and 181-1122C-1H, based on reflectance variability. The final composite section is illustrated in Figure F26.

Hole-to-hole correlation at the top of the sedimentary sequence, including determination of the mudline, presented a particular challenge at Site 1122. Core 181-1122C-1H is undoubtedly a mudline core, whereas Core 181-1122B-1H virtually filled the core liner. A thick sand recovered in Core 181-1122C-1H is represented by high MS and GRAPE density values. This sand was apparently washed out or disturbed in Hole 1122B, an inference based on anomalously low GRAPE density values near the equivalent depth of the sand layer in Core 181-1122B-1H. Excluding this sand layer, magnetic susceptibility and GRAPE density data do not vary enough to allow correlation. However, if one assumes that the top of Core 181-1122B-1H corresponds to the mudline recovered at the top of Core 181-1122C-1H, reflectance records agree well between Cores 181-1122B-1H and 181-1122C-1H. Based on reflectance data, we placed the top of Core 181-1122B-1H at the mudline. An alternative relationship, though less probable, is that the data from Core 181-1122C-1H represent an interval of strata recovered at some ill-defined level above the top of Core 181-1122B-1H. To calculate depths for this alternative relationship, 2.41 m has to be added to all mcd depths in Tables T10 and T11 (both also in ASCII format) except those depths for Core 181-1122C-1H. The relationship advocated here, with

F26. Composite sections, p. 68.



T10. Composite depth section, p. 131.

T11. Splice tie points, p. 138.

the mudline in both Cores 181-1122B-1H and 181-1122C-1H, places the Kawakawa Tephra at ~12.6 mcd in the splice in Core 181-1122A-H1 (Fig. F26).

Two coring irregularities occurred at Site 1122. First, Core 181-1122A-1H was shot when the end of the APC piston had already penetrated the topmost sediment by ~8 m, rather than close to the mudline. This large depth offset of Core 181-1122A-1H is based on convincing correlations via MS, GRAPE, and color reflectance. Additionally, the Kawakawa Tephra (Fig. F26) is found in both Holes 1122A and 1122C at levels agreeing with the composite section correlation (Fig. F26). Second, the top of Core 181-1122C-3H represents an interval that overlaps with the base of Core 181-1122C-2H, including a repeat recovery of the Kawakawa Tephra. The recoring of this interval may be related to advancing the drill string based on core recovery following retrieval of Core 181-1122C-2H.

Two correlations in the composite depth section are based on only small overlaps (1) between Cores 181-1122C-3H and 181-1122A-2H, and (2) between Cores 181-1122C-4H and 181-1122A-3H (Fig. F26). These correlations, based on GRAPE density records, are the least certain overlaps in the composite section. A definite gap exists between Cores 181-1122A-8H and 181-1122C-9H. In this case, we assigned the top of Core 181-1122A-8H a composite depth equal to the base of Core 181-1122C-9H.

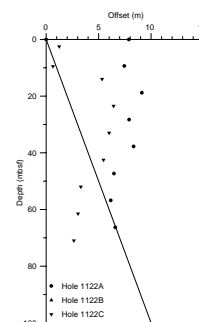
Downhole core offsets relative to mbsf depths do not follow a model of 10% stretch between the mbsf and mcd depth scales in the composite section. Instead the offset is ~6–8 m for the extent of Hole 1122A and 2–6 m in Hole 1122C below Core 181-1122C-3H (Fig. F27), with offsets following a slight negative slope below ~20 mbsf. Table T10 contains the offsets between the mbsf and mcd scales resulting from composite section construction.

The spliced record, based primarily on MS and GRAPE data (Fig. F28), extends to 83 mcd. Wherever possible, splice tie points (Table T11) were picked at well-defined maxima or minima where the overlap in data from Holes 1122B and 1122C are correlated. Typically, parameter values differed by less than 10% at tie levels. In all cases, ties were selected so that the spliced record was as free from noise (high-frequency variability) as possible.

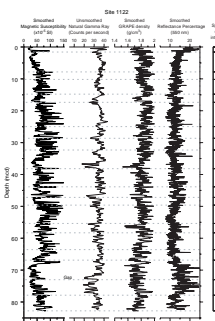
## AGE MODELS AND SEDIMENTATION RATES

Biostratigraphic levels with age significance at Site 1122 were derived from LO, FO, acme, LCO, and FCO events, using diatoms, radiolarians, nannofossils, and foraminifers. The 29 levels are shown in Table T8. To show the principal trends, the assembled age-depth data are plotted together with magnetic polarity datums in Figure F17. FO events may have been estimated to be too shallow, based on limited sampling. The position of arrows in Figure F17 reflects the possibility that further work may extend these datums downhole. Last occurrence events may be too deep, again as a result of the limited sampling interval. The position of arrows in Figure F17 reflects the possibility that further work may extend these datums uphole. The solid line in Figure F17 shows the preferred age depth model using magnetic polarity constrained by the biostratigraphic datums (see “Paleomagnetism,” p. 20). Given the fact that the sequence is dominated by turbidites down to ~400 mbsf, the scatter of event data is surprisingly low. Hence, average sedimenta-

F27. Downhole depth offsets, p. 70.



F28. Spliced record, p. 71.



tion rates may be expressed with relatively long linear segments. This observation suggests that any reworking of microfossil marker events was relatively instantaneous. An ~5-m.y. hiatus at 490 mbsf separates middle Miocene strata below from early Pliocene strata above. Below the hiatus, middle Miocene (compacted) sedimentation rates of lithostratigraphic Unit III and Subunit IIB were low, varying between 50 and 5 m/m.y. The late Miocene pelagic mud and laminated sand (contourite deposit), classified as the lower part of Unit IIA, has a much lower sedimentation rate of 2 m/m.y. Early Pliocene net sedimentation is also of low rate but poorly constrained. The sedimentation rate accelerated to ~100 m/m.y. from the latest Pliocene to early Pleistocene and became very fast (400 m/m.y.) in the middle and late Pleistocene when most of the Bounty Fan levee was deposited at this site.

Sediment decompaction and accumulation rates were assessed using 124 porosity measurements from Hole 1122C (see “[Physical Properties](#),” p. 32). These were analyzed for trends, using the programs DEPOR and BURSUB (Stam et al., 1987; Gradstein et al., 1989). Coarser grained lithostratigraphic Subunits IA, IB, IIIA, and IIIB were decompacted to a greater extent, relative to the middle, finer grained Subunits IC, ID, IIA, and IIB. Next, compacted and restored rates of sedimentation were derived, with the age intervals slightly smoothed; these are shown in Table T12. In lithostratigraphic Unit III, decompaction resulted in an 80% increase of rates, from 50 to 80 m/m.y. Decompaction had negligible effect on sedimentation rates of younger strata. This is in accord with the measured porosities in the basal siltstones, showing accumulation rate values ~60% lower than stratigraphically higher units. It must be remembered that this decomposition was performed on data from the preferentially preserved fine material; the coarse (and less compactible) sand turbidites were washed away during drilling or were not subjected to compression testing. The results in Table T12 are thus biased toward high values.

### Backtracking and Paleoceanography

The character of basement on multichannel seismic lines across Site 1122 and gravity and magnetic survey data (Davey, 1993; Carter et al., 1994) demonstrate that the distal part of the Bounty Trough is situated on oceanic crust in over 4 km of water. The abyssal ocean floor of the Bounty Fan is part of the most distal southwest Pacific Ocean, which started opening before marine magnetic Anomaly 32 (late Campanian) (Stock and Molnar, 1987). Anomaly 32 is mapped adjacent to Campbell Plateau, Bounty Trough, and Chatham Rise. The Bounty Fan Site 1122 itself is situated in the geomagnetic quiet zone, with an estimated age of ocean basement around 85 Ma (Lawver and Gahagan, 1994).

According to recent interpretations (Carter et al., 1994), the Bounty Trough is a failed and sediment-starved rift, at right angles to the Southwest Pacific Ocean spreading basin. The Bounty Trough lies between the continental blocks of Campbell Plateau to the south and Chatham Rise to the north. Drilling on the southern block has recovered a sequence of middle to upper Cretaceous coal measures and shallow marine terrigenous clastics, unconformably overlying metamorphic basement. Similar and coeval strata are inferred for the northern block (Raine et al., 1993). The Cretaceous sediments may be interpreted as synrift strata, formed during regional subsidence on a passive margin, adjacent to the rifted and opening Southwest Pacific Ocean.

---

T12. Compacted and restored rates of sedimentation, p. 139.

---

The thermal history of the distal Southwest Pacific oceanic crust constrains the subsidence history and sediment accommodation space at Site 1122. Figure F29 sketches the backtrack history, based on a ridge crest age at the location of Site 1122 at 85 Ma, which is slightly older than Anomaly 32, and on the observed present-day water depth at the site of nearly 4500 m. Initial ocean sediments at the site are postulated to be Late Cretaceous through Paleocene siliceous pelagic clays (see “**Lithostratigraphy**,” p. 3, in the “Site 1121” chapter). The presence of rare, reworked Oligocene nannofossils, diatoms, and planktonic foraminifers in middle Miocene strata at Site 1122 indicate that deep marine Oligocene strata also formed in the vicinity of the site. Regional sedimentation rate curves, considered representative for the Chatham Rise and part of the Campbell Plateau, show sustained sedimentation through the Late Cretaceous, reduced Paleocene–Eocene sedimentation, and a hiatus in the Oligocene through the early Miocene (fig. 3.2 in Wood et al., 1989). Hence, Oligocene fossils may have been transported from the New Zealand paleo-shelf.

From the seismic profile across Site 1122, the pre-middle Miocene ocean sediments are ~1 km thick. Figure F29 also shows the >130-m-thick middle Miocene marine silt and nannofossil ooze resting unconformably on older strata and the >490 m of uppermost Pliocene–Pleistocene fine sands and nannofossil ooze unconformably overlying the middle Miocene sediments. The rapid, late-stage sedimentation, beginning in the Miocene and steadily increasing thereafter, reflects the uplift of the Southern Alps in New Zealand. This shed an enormous volume of terrigenous material on the nascent shelf, slope, and rise to the east (Wood et al., 1989).

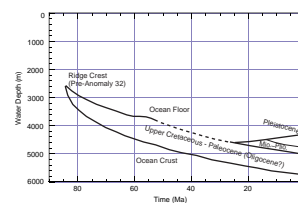
The combined evidence supports an oceanic history at the site that traces to ~85 Ma, pre-Anomaly 32 time. The abundance of shallow marine microfossils observed at some levels in the Pleistocene turbidites and middle Miocene drifts (see “**Biostratigraphy**,” p. 13) may be explained by geologic reworking, as part of the slow and inexorable fill of Bounty Trough, estimated to have taken at least 200 m.y. at the present rate of sedimentation (Carter et al., 1994).

## INORGANIC GEOCHEMISTRY

### Interstitial Water

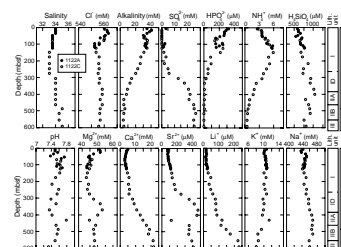
We collected interstitial water from 30 samples at Site 1122: 10 from Hole 1122A at depths ranging from 5.90 to 117.20 mbsf, and 20 from Hole 1122C at depths ranging from 67.40 to 591.80 mbsf (Table T13, also in **ASCII format**). One interstitial-water sample was taken from each core in the upper 100 mbsf. From 100 mbsf to the bottom of the hole, every third core was sampled. Samples from Holes 1122A and 1122C are plotted together in Figure F30. Stratigraphic correlation based on high-resolution data of magnetic susceptibility, GRAPE density, and spectral reflectance demonstrate that ~8 m of the upper part of Hole 1122A are missing (see “**Composite Depths**,” p. 24). Comparison between the interstitial-water concentrations of the first sample of Hole 1122A and normal seawater values supports this conclusion. In general, the concentrations of the uppermost samples are close to the seawater composition because of the dominant water exchange at the seawater-sediment interface. The uppermost sample of Hole 1122A (5.90 mbsf) shows a large offset from the seawater values, suggesting that it origi-

F29. Sketch of oceanic subsidence history of Site 1122, Bounty Fan, p. 72.



T13. Summary of interstitial-water geochemistry, p. 140.

F30. Depth profiles of interstitial-water constituents at Site 1122, p. 73.



nated from a depth greater than 5.90 mbsf (see “[Composite Depths](#),” p. 24).

### Salinity, Chloride, pH, and Sodium

Salinities of the interstitial-water samples show a decreasing trend from 5.95 to 272.70 mbsf, and then remain virtually constant down to 460.30 mbsf (Fig. [F30](#)). The salinity decrease results from the removal of sulfate by bacterial reduction. The local maximum (35.0) was found at 487.40 mbsf. The salinity increase in the lower part of Hole 1122C reflects the enrichment of major ion concentrations including calcium, magnesium, and sodium, as described below.

The chloride ( $\text{Cl}^-$ ) concentration shows a small increase from 560 mM at 5.90 mbsf to the maximum (563 mM) at 34.20 mbsf (Fig. [F30](#)), then decreases to 554 mM at 147.90 mbsf and remains between 555 and 559 mM to the bottom of the hole. The chloride decrease seems to parallel the behavior of salinity, which has also been observed at Site 1119 (see “[Inorganic Geochemistry](#),” p. 21, in the “Site 1119” chapter). However, the reduction of chloride may not be caused by the fresh-water input, but is probably the result of charge balance control accompanied by complete sulfate utilization.

Interstitial water pH values show a highly variable pattern, ranging from 7.32 to 7.79 (Fig. [F30](#)). The highest pH (7.79) occurs at 431.40 mbsf, which coincides with the concentration anomalies of magnesium, strontium, potassium, and silica.

Concentrations of sodium ( $\text{Na}^+$ ) follow a similar trend to the chloride concentrations and vary from 438 to 468 mM (Fig. [F30](#)).

### Alkalinity, Sulfate, Ammonium, and Phosphate

Alkalinity, sulfate, phosphate, and ammonium concentrations are strongly controlled by the availability of organic matter for bacterial degradation. The alkalinity of interstitial water decreases with depth down to 431.40 mbsf and remains almost constant toward the bottom of the hole (Fig. [F30](#)). The small variation at ~100 mbsf is caused by the depth offset between Hole 1122A and Hole 1122C (see “[Composite Depths](#),” p. 24). The alkalinity maximum at 15.20 mbsf represents the interval of the most intense sulfate reduction. The increase in alkalinity is the result of the production of bicarbonate during bacterial degradation of organic matter, primarily by sulfate reduction. The almost constant alkalinity between 45.10 and 147.90 mbsf coincides with complete sulfate reduction and the onset of methanogenesis. The linear decrease in alkalinity down to 431.40 mbsf presumably is caused by carbonate recrystallization and/or silicate reconstitution processes, which use the bicarbonate ion from interstitial water (Gieskes, 1974).

The sulfate ( $\text{SO}_4^{2-}$ ) concentration decreases from 3.3 mM at 5.90 mbsf to 0 mM between 15.20 and 122.00 mbsf, followed by an increase to ~26.5 mM at 514.80 mbsf (Fig. [F30](#)). Below this depth, sulfate remains almost constant. The sulfate profile is governed by several factors, of which the most important are the abundance (and/or availability) of organic matter and the sedimentation rate. Bacterially controlled sulfate reduction processes have completely depleted sulfate in the pore waters down to ~150 mbsf, resembling nearshore settings with high organic carbon contents and higher bulk accumulation rates such as the Gulf of California (Gieskes et al., 1982) or the Peruvian margin (Suess, von Huene, et al., 1988). The complete utilization of sulfate in